Mechanical behavior and deformation micromechanisms of polypropylene nonwoven fabrics as a function of temperature and strain rate

R. Jubera , A. Ridruejo , C. González , J. LLorca

A B S T R A C T

The mechanical behavior and the deformation and failure micromechanisms of a thermally-bonded polypropylene nonwoven fabric were studied as a function of temperature and strain rate. Mechanical tests were carried out from 248 K (below the glass transition temperature) up to 383 K at strain rates in the range $\approx 10^{-3}\,s^{-1}$ to $10^{-1}\,s^{-1}$. In addition, individual fibers extracted from the nonwoven fabric were tested under the same conditions. Micromechanisms of deformation and failure at the fiber level were ascertained by means of mechanical tests within the scanning electron microscope while the strain distribution at the macroscopic level upon loading was determined by means of digital image correlation. It was found that the nonwoven behavior was mainly controlled by the properties of the fibers and of the interfiber bonds. Fiber properties determined the nonlinear behavior before the peak load while the interfiber bonds controlled the localization of damage after the peak load. The influence of these properties on the strength, ductility and energy absorbed during deformation is discussed from the experimental observations.

1. Introduction

Textile materials have greatly benefited from the advances in fiber technology. Woven textiles are the natural choice when design specifications require high performance in terms of strength and stiffness. Moreover, their regular pattern makes it easier to model the relationship between the microstructure and the macroscopic behavior. Recent investigations (Lomov et al., 2007; Boubaker et al., 2007; Cao et al., 2008; Badel et al., 2008; Khan et al., 2010; Durville, 2010) have contributed to a deeper understanding of the mechanical behavior of woven textiles. Nevertheless, knitted and nonwoven fabrics provide better performance if the goal is deformability and energy absorption. Knitted materials also exhibit a regular structure based on loops and knots which leads to costly manufacturing processes. Processing of nonwoven fabrics (or simply nonwovens) is significantly cheaper, since they are manufactured from disordered fibers which are consolidated by means of chemical binding, local thermal fusion or mechanical entanglement. The variability in fibers and bonding techniques leads to a wide range of properties and microstructural randomness accounts for a distinctive complex mechanical behavior. An increasing number of applications take advantage of the versatileness of nonwovens, including filters, geotextiles, fuel cell membranes or fabrics for ballistic protection, to name but a few (Russell, 2007).

Despite of the complexity of the deformation and damage mechanisms in nonwovens (or perhaps due to this factor), several models of the mechanical behavior have been recently developed. They address different

micromechanisms of deformation and fracture typical of nonwovens, such as straightening of curved fibers, large deformations and extensive fiber rotation, topology changes due to bond breakage, fiber sliding and fracture, etc. (Hou et al., 2009, 2011; Ridruejo et al., 2010, 2012; Silberstein et al., 2012; Kulachenko and Uesaka, 2012; Wilbrink et al., 2013). However, experimental studies that relate the microstructure with the failure micromechanisms and properties have been limited to paper (Bronkhorst, 2003; Hägglund and Isaksson, 2006; Isaksson et al., 2006, 2004). In fact, most of the available experimental information of the mechanical behavior of nonwovens comes from the manufacturers' data sheets, which typically emphasize performance and provide very limited information about the fabric structure and its deformation and fracture mechanisms. Experimental studies focused on the characterization of the micromechanisms of deformation and fracture of nonwovens appeared only very recently (Rawal et al., 2008; Isaksson and Hägglund, 2009; Ridruejo et al., 2010, 2011; Isaksson et al., 2012), and they often use state-of-the-art characterization techniques (e.g. *in situ* testing within the scanning electron microscope, X-ray microtomography, digital image correlation) to establish the sequence of deformation and fracture events at the μm level.

It is obvious that further optimization of nonwoven textiles as well as validation of models require a deeper understanding of the microstructure-mechanisms-properties relationship and this was the main goal of this investigation. The material selected was a thermally-bonded polypropylene nonwoven, commercially available as a geotextile. This class of materials stands out because of its excellent strength and energy absorption capability (Rawal et al., 2010; Ridruejo et al., 2011; Farukh et al., 2013). Mechanical characterization was carried out at temperatures above and below the glass transition temperature and near to the melting point to assess the influence of fiber properties on the mechanical behavior and at strain rates in the range 10^{-3} to 10^{-1} s^{-1}. Different experimental techniques (including *in situ* testing within the scanning electron microscope and digital image correlation) were used to analyze the deformation and damage mechanisms as a function of temperature and strain rate. Individual fibers, extracted from the nonwoven fabric, were also tested under the same conditions. The result of this comprehensive characterization provided a detailed picture of the dominant deformation and fracture mechanisms as a function of the temperature and strain rate and their influence on the macroscopic properties (namely strength and energy absorption). Moreover, this comprehensive characterization of the mechanical behavior at different strain rates and temperatures can be used as a benchmark for the calibration of constitutive models for this type of materials.

2. Material and experimental techniques

2.1. Polypropylene nonwoven fabric

The nonwoven material under study was a geotextile made of polypropylene fibers (commercial trade name Typar SF32) manufactured by Du Pont de Nemours. The isotactic polypropylene (PP) fibers were extruded and then stretched to increase crystallinity, resulting in fibers of 40–60 μm in diameter, 0.91 g/cm^3 of density, 48% crystallinity and 438 K of melting temperature (Fig. 1) Ridruejo et al., 2011; Jubera, 2013. The continuous spun fibers were laid down randomly on a flat surface producing an isotropic fiber web sheet which was then bonded by the simultaneous application of pressure and heat. The fibers typically appear as isolated, although bundles of 2–5 fibers were often found (Fig. 1). Partial fusion between fibers at the entanglement points was normally observed. Differential scanning calorimetry tests confirmed that the melting temperature and the crystallinity of the PP in the thermal bonds were below that of the fibers. The processing route leads to a nonwoven with a random fiber distribution and isotropic properties (Ridruejo et al., 2011; Jubera, 2013).

2.2. Fiber mechanical characterization

Individual fibers were extracted from the nonwoven fabric by carefully pulling with tweezers. Fibers with a gage length of in the range 4.9 to 6.1 mm were stitched on a cellulose acetate frame, which was fixed to a mechanical testing machine for the tensile tests. The load was exerted on the fiber after cutting the cardboard. The experimental set-up was located within an environmental chamber and mechanical tests were carried out at 248, 298 and 383 K. The temperature of 248 K was selected because it was well below the glass transition temperature of the PP, which was found to be around 283 K by differential scanning calorimetry Jubera, 2013. The fiber temperature during the tests was measured with a thermocouple very close to the fiber.

Tensile tests were carried out at constant cross-head displacement. Fiber elongation was determined as the cross-head displacement, since the machine compliance was negligible as compared with the fiber. Tests were carried out at three different strain rates of 8.0×10^{-4}, 8.0×10^{-3} and 10^{-1} s^{-1}. The load carried by the fibers was measured by using a load cell with ±1 mN resolution.

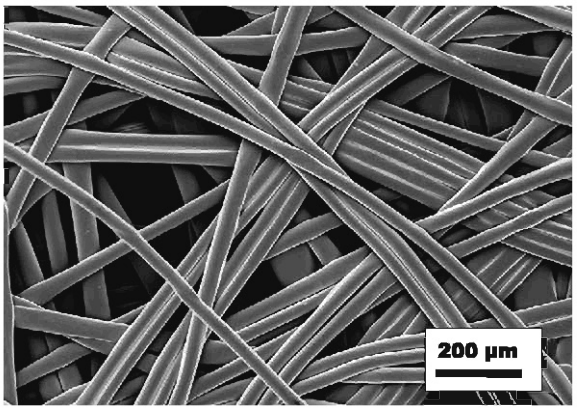

Fig. 1. Scanning electron micrograph of the PP nonwoven fabric Typar SF32, manufactured by Du Pont de Nemours.

Engineering strains were computed as the fiber elongation divided by the initial length. Nominal stresses were obtained from the load and the initial fiber diameter, assuming a circular section. The fiber diameter was accurately measured in profile projector prior to testing.

2.3. Nonwoven fabric mechanical characterization

Rectangular coupons of 150 mm in height and 100 mm in width, following EN ISO 10319 standard, were cut from the rolls to measure the mechanical properties under uniaxial tension. The areal density of the nonwoven textile, as determined from the coupon weight and area, was 111 ± 2 g/cm^2. Special grips made of two steel beams with a canal were used to load the specimens. The grips were connected to the actuator of the mechanical testing machine through a mechanical hinge to eliminate bending stresses. The ends of the coupon were inserted into the canal and clamped between two steel plates protected with rubber to prevent damage to the fabric. The clamping force was exerted by bolts distributed along the beam. The steel grips were connected to the actuator and the load cell of the mechanical testing machine. The initial coupon length between grips was 100 mm.

Tests were carried out under stroke control at crosshead speeds of 0.08, 0.8 and 10 mm/s, which lead to average strain rates of 8.0×10^{-4}, 8.0×10^{-3} and 10^{-1} s^{-1}. The load was continuously measured with a 5 kN load cell. The experimental set-up was placed within an environmental chamber and the mechanical tests were carried out at 248, 298 and 383 K. The temperature within the chamber was controlled by means of two thermocouples. The environmental chamber had a glass window and the deformation pattern on the specimen surface was obtained by means of digital image correlation using commercial software (VIC 2D) in the tests carried out at ambient and increased temperature (Totry et al., 2009, 2010). Water condensation on the glass and inside the chamber hindered the use of this technique at 248 K.

2.4. In situ mechanical characterization

Small coupons of 24 mm in height and 6 mm in width were used to study damage micromechanisms at the fiber level. To this end, the coupon was coated with Au by sputtering and clamped by screwing steel plates to the yokes attached to the load cell and actuator of a micro-electromechanical testing machine (Kammrath & Weiss) inside a

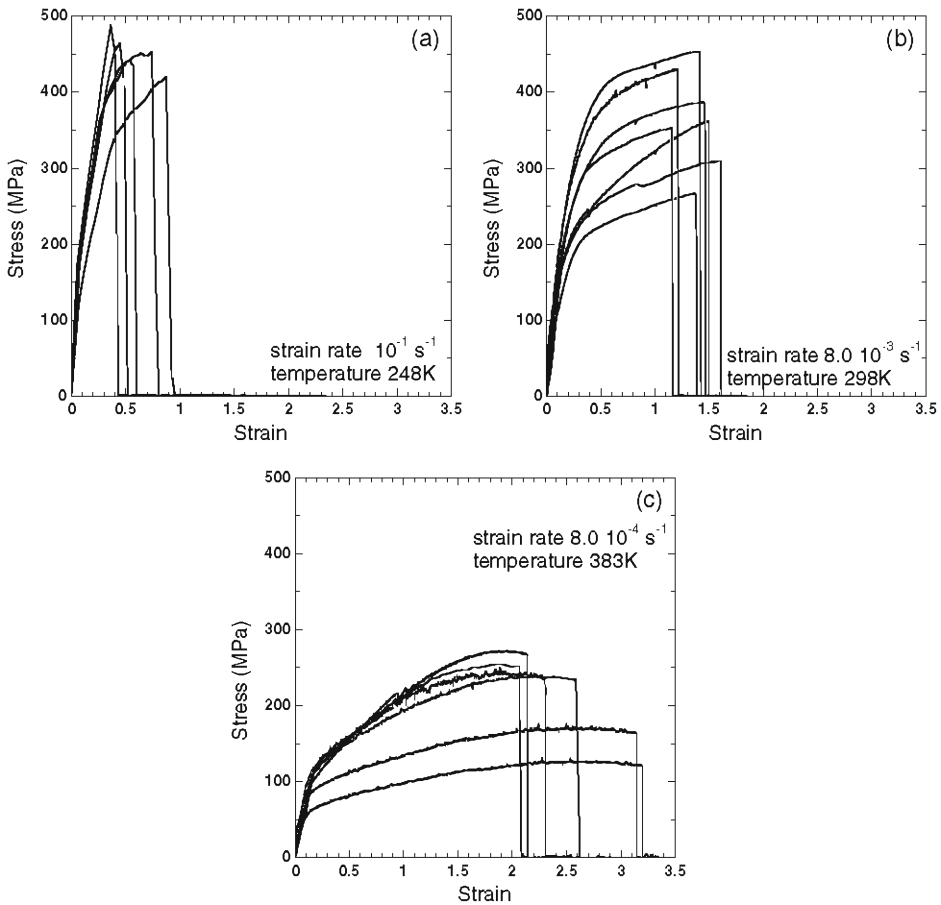

Fig. 2. Tensile engineering stress *vs.* engineering strain curves of PP fibers at different strain rates and temperatures. (a) Average strain rate 10^{-1} s^{-1}, temperature 248 K. (b) Average strain rate 8.0×10^{-3} s^{-1}, temperature 298 K. (c) Average strain rate 8.0×10^{-4} s^{-1}, temperature 383 K.

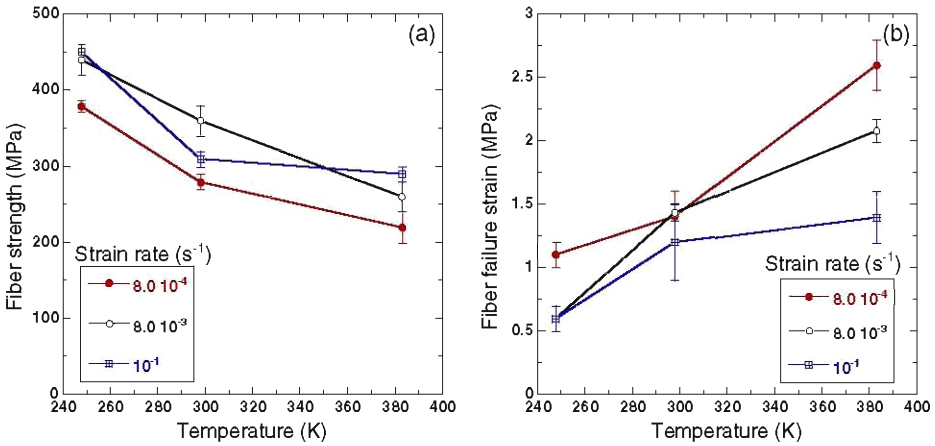

Fig. 3. (a) Influence of temperature on the tensile strength of PP fibers tested at different strain rates. (b) Influence of temperature on the failure strain of PP fibers tested at different strain rates.

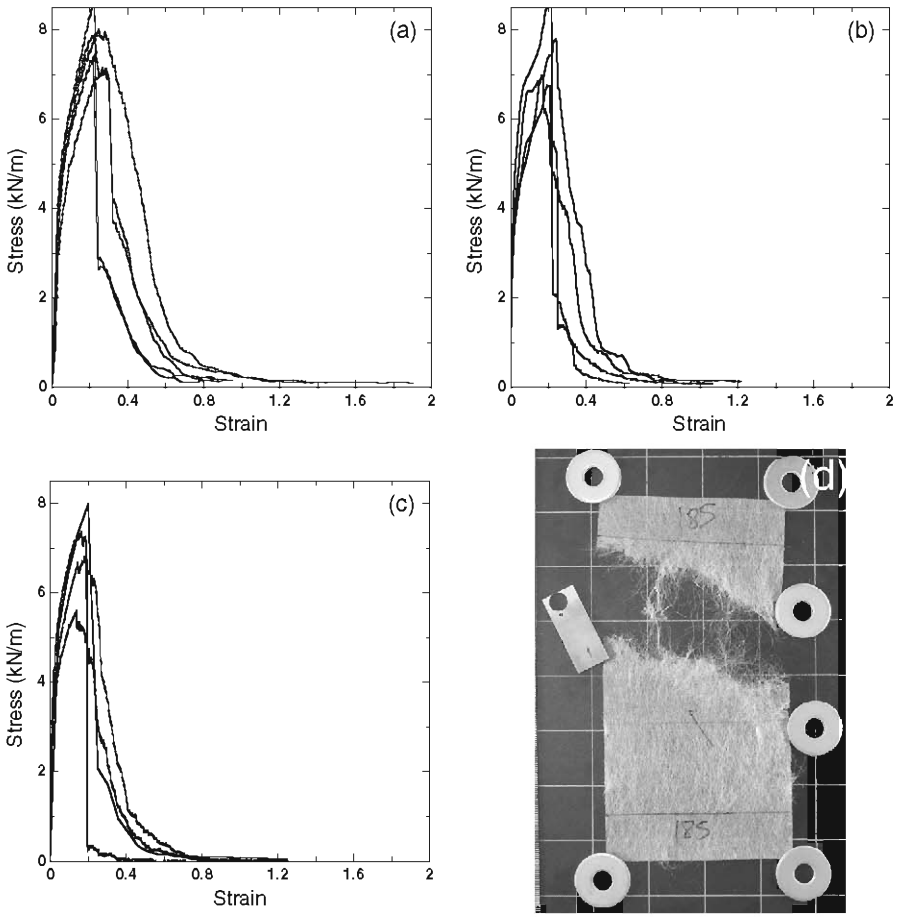

Fig. 4. Evolution of nominal stress *vs.* engineering strain in the square specimens loaded in tension at 248 K. (a) Average strain rate of $8.0 \times 10^{-4}\,s^{-1}$. (b) Average strain rate of $8.0 \times 10^{-3}\,s^{-1}$. (c) Average strain rate of $10^{-1}\,s^{-1}$. (d) Broken specimen after deformation at $8.0 \times 10^{-3}\,s^{-1}$. The dimensions of the background square pattern are 30 × 30 mm.

scanning electron microscope. The testing area for the specimen was 18 × 6 mm and it was loaded in tension at a cross-head speed of 0.01 mm/s, which led to an approximate strain rate of $5.6 \times 10^{-4}\,s^{-1}$. Tests were carried out at 298 and 383 K. Micrographs of the deformed fabric were taken at different magnification levels to assess the micromechanisms of deformation and fracture as a function of strain and temperature. Load was not recorded because no actual load signal could be distinguished from the background noise, given the fact that the load cell was designed for a maximum load of 10 kN.

3. Fiber properties

The mechanical properties of the PP fibers were measured at three different temperatures and strain rates. Out of these nine set of experiments, representative engineering strain *vs.* engineering strain curves of three of them are plotted in Fig. 2. Fig. 2(a) includes the tests carried out at the highest strain rate ($10^{-1}\,s^{-1}$) and the lowest temperature (248 K). Fig. 2(b) depicts the curves obtained at an intermediate strain rate ($8.0 \times 10^{-3}\,s^{-1}$) and 298 K, while the data corresponding to the lowest strain rate ($8.0 \times 10^{-4}\,s^{-1}$) and the highest temperature (383 K) are depicted in Fig. 2(c). Regardless of the differences in strain rate and temperature, all the curves presented an initial elastic region, followed by a non-linear zone which ends with the sudden fracture of the fiber. However, the initial flow stress decreased and the strain-to-failure increased rapidly with temperature (particularly at 383 K) as a consequence of the thermal activation of viscoplastic deformation mechanisms in PP. The experimental scatter was large and the main cause was probably the variations in the fiber section along its length. Nevertheless, damage and plastic yielding introduced in the fibers during the extraction from the nonwoven fabric cannot be ruled out.

The influence of temperature and strain rate of the mechanical properties of the fibers is summarized in Fig. 3. They show that the fiber strength decreased rapidly with temperature while the failure strain increased with temperature. The influence of the strain rate on the mechanical properties was limited, particularly at 248

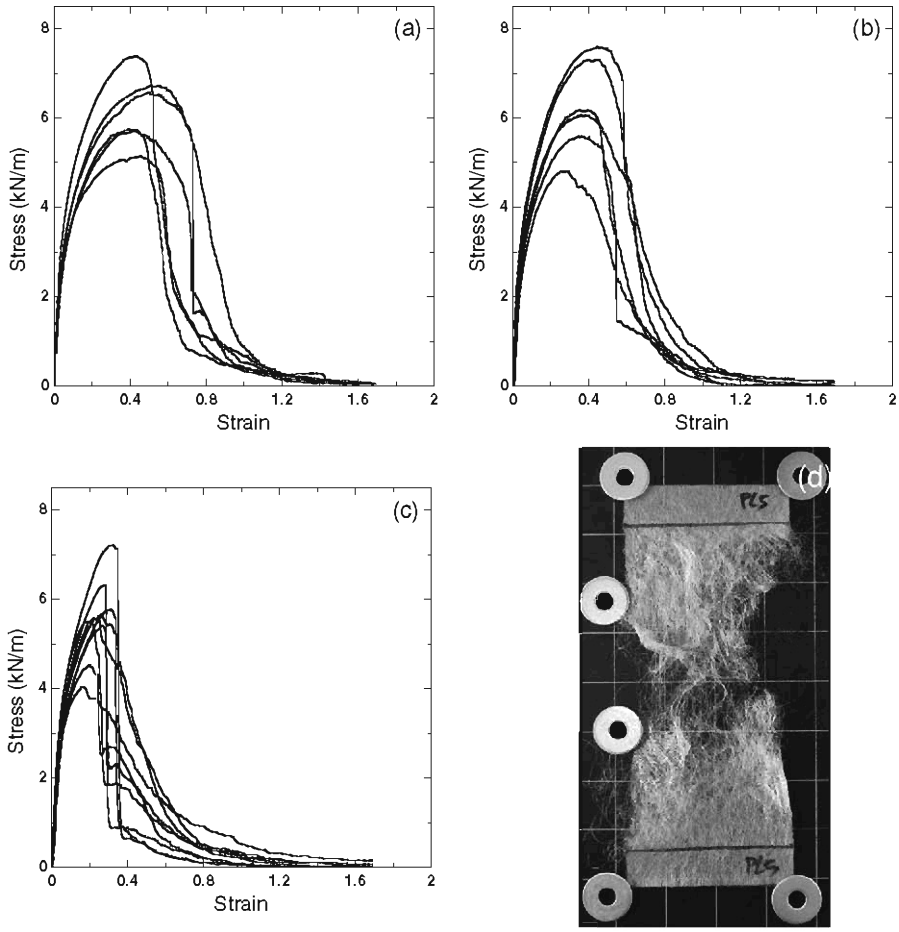

Fig. 5. Evolution of nominal stress *vs.* engineering strain in the square specimens loaded in tension at 298 K. (a) Average strain rate of $8.0 \times 10^{-4}\,s^{-1}$. (b) Average strain rate of $8.0 \times 10^{-3}\,s^{-1}$. (c) Average strain rate of $10^{-1}\,s^{-1}$. (d) Broken specimen after deformation at $8.0 \times 10^{-3}\,s^{-1}$. The dimensions of the background square pattern are 30 × 30 mm.

and 298 K. Fibers tested at low strain rates showed much higher ductility (and lower strength) than those tested at high strain rate only at 383 K.

4. Nonwoven fabric properties

The mechanical properties under tension of the PP nonwoven fabric were measured as a function of strain rate and temperature. An average of six tests were carried out for each temperature and strain rate to account for the inherent statistical variability in the mechanical behavior of these materials. The evolution of nominal stress (expressed in terms of force per unit width) as a function of the engineering strain is plotted in Figs. 4–6, which include the results of the tests carried out at 248, 298 and 383 K, respectively. In addition, Fig. 4(a–c) contain the curves obtained at average strain rates of 8.0×10^{-4}, 8.0×10^{-3} and 10^{-1} s^{-1}, respectively, and similar results are presented in Figs. 5 and 6 at higher temperatures. Pictures of the failed specimens are also depicted in Figs. 4(d), 5(d) and 6(d).

Regardless of the temperature and strain rate, all curves present a number of common features. They include an initial linear zone, followed by a nonlinear regime, which led to a maximum in the load-carrying capability of the nonwoven fabric. Two different regimes were found after the peak even among specimens tested under the same conditions of strain rate and temperature. The first one was characterized by a gradual reduction of the stress borne by the fabric, while the second presented one (or, sometimes, two) abrupt reductions in stress, associated to the sudden localization of damage. The nominal stress–strain curve normally ended with a very long tail as the nonwoven fabric was able to transmit stresses at large engineering strains.

The effect of the temperature on the shape of the stress–strain curve is made evident by comparing the curves in Figs. 4–6. The ductility of the PP nonwoven fabric below the glass transition temperature was greatly reduced, both in terms of the strain at maximum load and of the strain at complete failure (when the load carried by the fabric reached zero). Moreover, most of the stress–strain curves at 248 K showed a marked drop in stress after the peak load. This was indicative of failure by localization of fracture in a given section of the fabric, with very little damage outside this region. This is clearly seen in the photograph of a specimen broken at 248 K and the

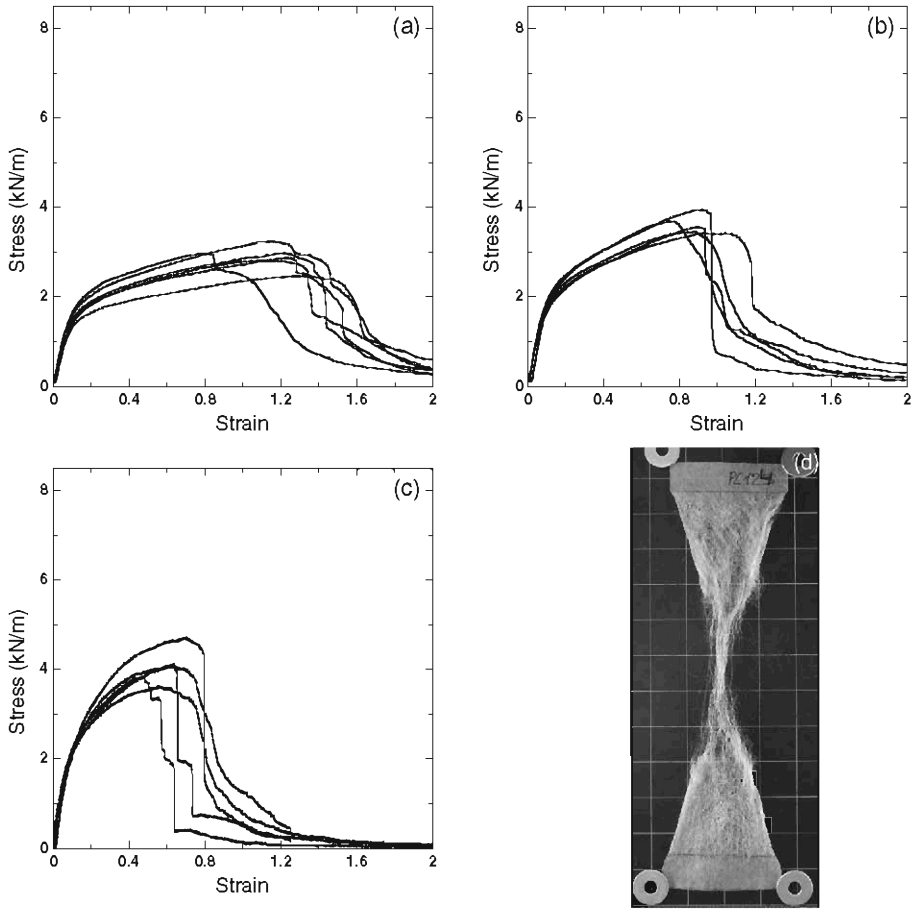

Fig. 6. Evolution of nominal stress *vs.* engineering strain in the square specimens loaded in tension at 383 K. (a) Average strain rate of 8.0×10^{-4} s^{-1}. (b) Average strain rate of 8.0×10^{-3} s^{-1}. (c) Average strain rate of 10^{-1} s^{-1}. (d) Broken specimen after deformation at 8.0×10^{-3} s^{-1}. The dimensions of the background square pattern are 30 × 30 mm.

intermediate strain rate: damage was concentrated in a very narrow strip above and below the fracture plane.

The tests carried out at 298 K, above the glass transition temperature of PP, showed a more ductile behavior. The nonlinear region before the peak load was longer and many specimens showed a gradual reduction in the load-bearing capacity after the peak (Fig. 5(a) and (b)) except in the tests carried out at high strain rate. As a result, the strain at maximum load and the strain at complete failure increased with respect to those measured at 248 K. Damage was not localized above and below the fracture surface but it was spread throughout the sample, as shown in the photograph of a broken specimen (Fig. 5(d)).

Finally, the specimens tested at 383 K showed a marked reduction in strength while the strain at maximum load and the strain at complete failure increased dramatically (Fig. 6(a–c)). Damage prior to failure was spread throughout the whole specimen and final failure did not take place by the localization of damage in a fracture plane but by progressive necking of the specimen up to the formation of a thin filament as a result of the disentanglement and progressive alignment of the fibers (Fig. 6(d)). Complete specimen fracture was not attained because the actuator reached its maximum displacement.

The influence of temperature and strain rate on the nominal strength of the PP nonwoven fabrics is summarized in Fig. 7. Overall, strength decreased linearly with temperature and the lower the strain rate, the higher the strength reduction (Fig. 7(a). The influence of the strain rate on the nominal strength was more limited and it was negligible at 298 K (Fig. 7(b)). Strength decreased slightly with strain rate in specimens tested below the glass transition temperature, while the opposite trend was found in the specimens tested at 383 K.

The energy absorption capability of the nonwoven fabric as a function of temperature and strain rate is plotted in Fig. 8(a) and (b), respectively. It was determined from the area under the force *vs.* displacement curves and provides an indication of the ductility of the material. While strength was mainly controlled by

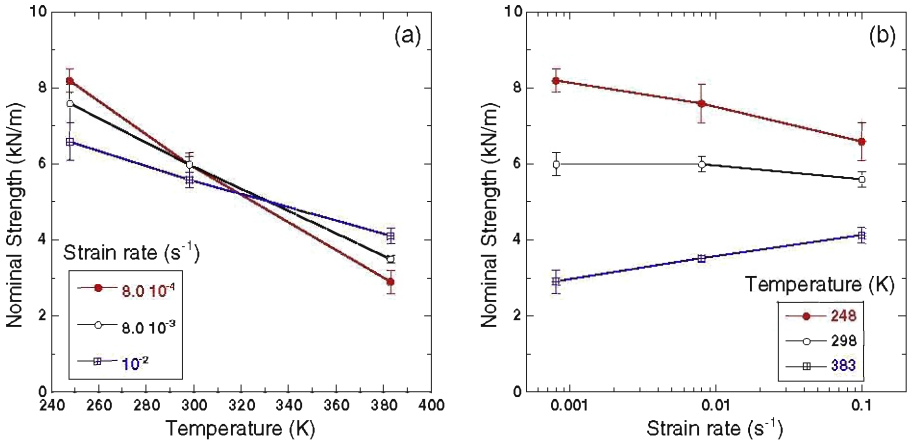

Fig. 7. (a) Influence of temperature on the nominal strength of PP nonwoven fabrics tested at different strain rates. (b) Influence of strain rate on the nominal strength of PP nonwoven fabrics tested at different temperatures.

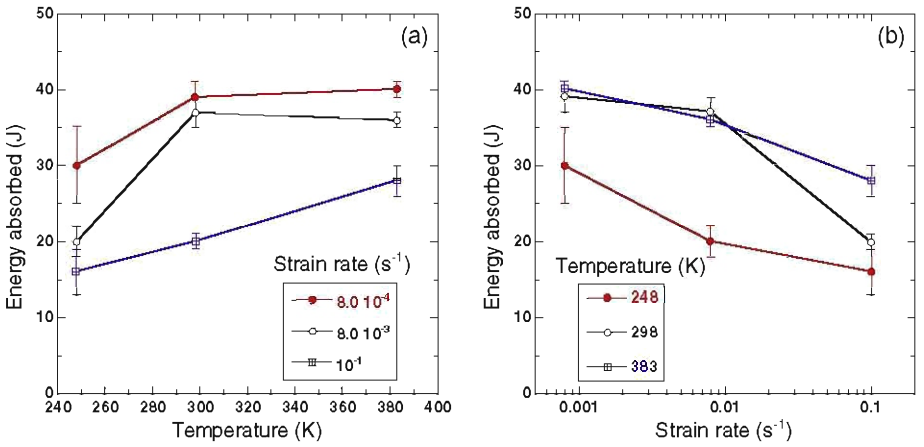

Fig. 8. (a) Influence of temperature on the energy absorbed during tensile deformation of PP nonwoven fabrics tested at different strain rates. (b) Influence of strain rate on the energy absorbed during tensile deformation of PP nonwoven fabrics tested at different temperatures.

temperature, strain rate only played a secondary role, the energy absorbed during tensile deformation was equally dependent on both parameters. Increasing temperature or decreasing the strain rate led to a notable increase in the energy absorbed during fracture and also in the strain at the maximum strength (not plotted for the sake of brevity).

5. Micromechanisms of deformation and fracture

In order to understand the micromechanisms of deformation and failure as a function of temperature and strain rate, two experimental techniques were used. The first one was to carry out mechanical tests within the scanning electron microscope, so that the micromechanisms of

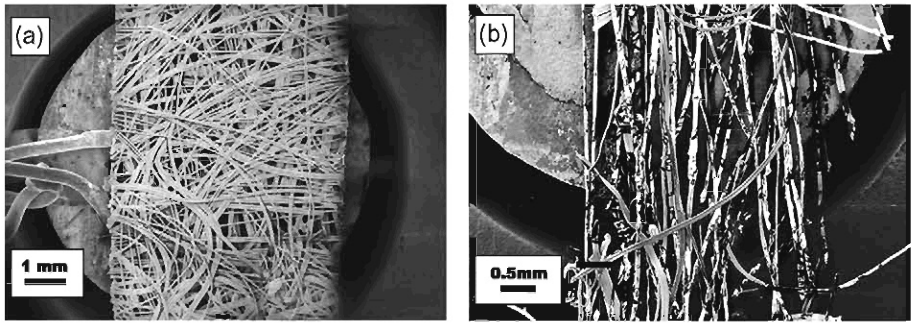

Fig. 9. Central region of the nonwoven specimen tested within the scanning electron microscope at 298 K. (a) Before testing. (b) At the end of the test when the applied engineering strain was 0.49. Loading direction was vertical.

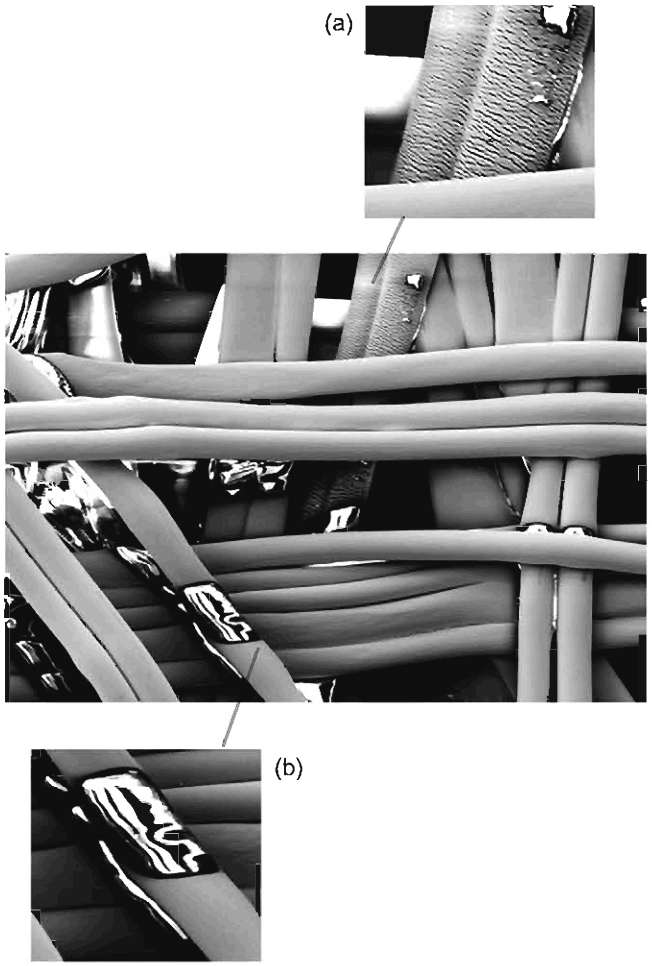

Fig. 10. Deformation and failure mechanisms at 298 K in the PP nonwoven fabric. (a) Detail of the fiber surface showing the cracking of the Au coating as a result of plastic deformation of the fiber. (b) Detail of interfiber bond fracture. The applied engineering strain was 0.49. Loading axis was vertical.

deformation and fracture at the fiber level could be ascertained from the qualitative viewpoint. It should be noticed that the overall macroscopic behavior of these samples was conditioned by the small specimen dimensions because fibers oriented along the loading direction were clamped on both ends and could not rotate. In addition, fibers perpendicular to the loading axis were shorter, presented fewer bonding points and could rotate more easily. Micrographs prior to testing (Fig. 9)(a) and at the end of the test (Fig. 9(b)) showed extensive fiber orientation upon deformation. Micrographs at higher magnification obtained at the early stages of deformation showed the two main deformation mechanisms, namely interfiber bond fracture and plastic deformation of the fibers oriented along the loading direction (Fig. 10). Plastic deformation of fibers was revealed by the cracking of the sputter-deposited Au coating while interfiber fracture surfaces were bright due to the electrical charging of the PP. Previous investigations have shown that interfiber bond fracture starts at very low strain (a few percents) at ambient temperature (Ridruejo et al., 2011), leading to a rearrangement of the fiber orientation and to a reduction in the fabric stiffness. Mechanical testing within the scanning electron microscope at high temperature showed the same

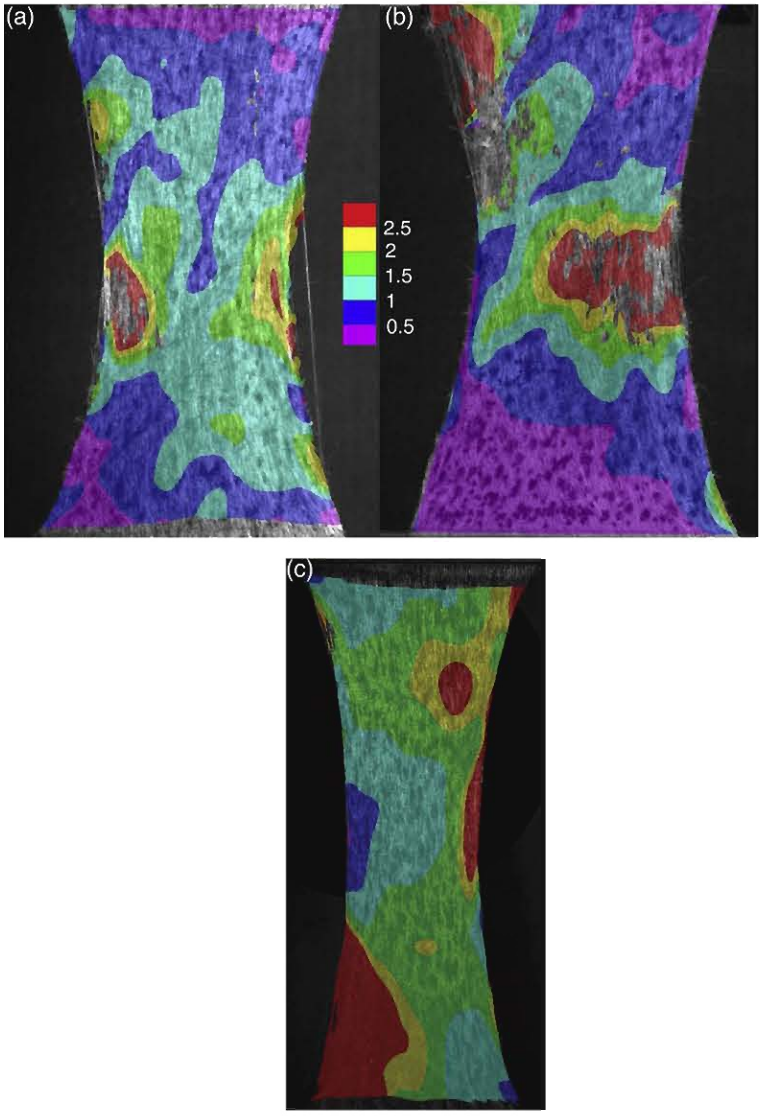

Fig. 11. Contour plot of the engineering strain in the loading direction in nonwoven fabrics tested at an average strain rate of $8.0 \times 10^{-4}\,s^{-1}$. (a) Test temperature of 298 K and applied engineering strain of 0.74. (b) Test temperature of 298 K and applied engineering strain of 0.72. (c) Test temperature of 383 K and applied engineering strain of 1.22.

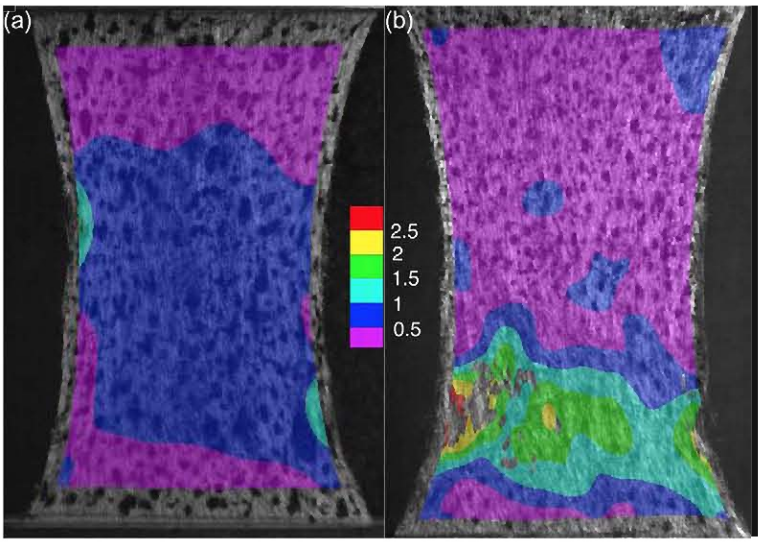

Fig. 12. Contour plot of the engineering strain in the loading direction in a nonwoven fabric tested at an average strain rate of $8.0 \times 10^{-3}\,s^{-1}$ and 298 K. (a) Applied engineering strain of 0.45. (b) Applied engineering strain of 0.52.

deformation and failure mechanisms, although plastic yielding of fibers and bonds was enhanced. The corresponding micrographs are not included for the sake of brevity.

Regarding the macroscopic behavior of the nonwoven fabrics, these processes (bond breakage and fiber reorientation) were the main mechanisms responsible for the nonlinear behavior observed in the stress–strain curves of the PP nonwoven fabrics at different strains rates and temperatures (Figs. 6–8). The maximum load was attained under these conditions without any evidence of fiber fracture because the failure strain of the fibers (Fig. 3(b)) was always much higher that the strain at maximum load in the nonwoven fabric tested under equivalent conditions of strain rate and temperature. Nevertheless, fibers initially oriented in the loading direction underwent plastic deformation, and this mechanism also contributed to the nonlinearity in the stress–strain curve, particularly in the fabrics tested at high temperature.

In the test carried out at 248 K, failure occurred by the localization of damage after the peak load (Fig. 4). A similar behavior was found at 298 K in the samples tested at high strain rates (Fig. 5(c)), while damage was spread throughout the specimen and the load decreased slowly with the applied strain at low strain rates (Fig. 5(a) and (b)). The onset of strain localization in the specimens tested at 298 and 383 K could be analyzed from the strain field maps obtained by digital image correlation. The contour plots of the vertical strain in two nonwoven fabrics tested at 298 K and low strain rate ($8.0 \times 10^{-4}\,s^{-1}$) are plotted in Fig. 11(a) and (b). The far-field applied strain was very similar in both cases (0.72–0.74) and larger than the strain at maximum load (Fig. 5(a)). The grey regions in Fig. 11(a) and (b) correspond to zones of maximum damage, in which the digital image correlation algorithm was not able to track the displacement field. These regions had sparse density and the fibers were oriented along the loading axis. Both figures show that damage localization was not concentrated in a narrow section but was rather spread throughout the sample. This is indicative of widespread interfiber bond fracture during deformation, which led to a diffuse damage pattern. Strain concentration at the center of the specimen because of geometrical considerations led to the final localization of damage at strains much larger than the strain at maximum load.

The diffuse damage pattern is more evident in Fig. 11(c), which depicts the contour plot of the engineering strain in the specimen tested at 383 K and low strain rate ($8.0 \times 10^{-4}\,s^{-1}$). While the far-field applied strain was 1.22, there are several regions throughout the sample in which the local strain was larger than 2.5. Widespread interfiber bond fracture at high temperature led to the progressive disentanglement of the fiber network and there was no damage localization. Final fracture occurred by the necking of the specimen up to the formation of a thin filament, as shown in Fig. 6(d).

The contour plots of the vertical strain prior to the maximum load are plotted in Fig. 12 for a nonwoven fabric tested at 298 K and intermediate strain rate ($8.0 \times 10^{-3}\,s^{-1}$), which presented damage localization. The strain distribution in the central region of the specimen was homogeneous at an applied strain of 0.45, prior to the maximum load (Fig. 12(a)). However, strain localization in a given section developed rapidly after the peak load and it was fully developed at an applied strain of 0.52 (Fig. 12(b)). The strains in the rest of the sample, outside of the localization band, decreased and the specimen failed immediately. This process was more abrupt in the case of the specimens tested at the highest strain rate and it was not possible to capture the strain map after the onset of localization. It is obvious that interfiber bond fracture under these conditions started in a given section

and propagated very rapidly across the specimen, as opposed to the widespread damage found at high temperatures and low strain rates.

6. Concluding remarks

The deformation and failure micromechanisms and their influence on the macroscopic tensile properties were studied in a thermally-bonded PP nonwoven fabric in a wide range of temperatures and strain rates. The onset of damage at the fiber level was ascertained by means of mechanical tests within the scanning electron microscope, while the evolution of strain fields obtained by digital image correlation provided information about the onset of localization at the macroscopic level. In addition, individual fibers extracted from the fabric were tested under the same conditions.

Damage began in all cases by the fracture of interfiber bonds, leading to a re-arrangement of the fiber orientation within the fabric. The maximum load was attained before fiber fracture in the whole range of temperatures and strain rates and the post-peak behavior depended on the loading conditions. At low temperature (248 K, below the glass transition temperature of PP), the nonlinearity in the stress–strain curve was limited, following the fiber behavior. Fracture was always brittle after the maximum load was attained and occurred by the localization of damage in a section of the specimen. This process was likely triggered by the brittle fracture of the interfiber bonds below the glass transition temperature. As a result of these mechanisms, nonwoven fabrics tested below the glass transition temperature presented higher strength and lower energy absorption capabilities.

On the contrary, nonwoven fabrics tested at high temperature (383 K) presented an extremely ductile behavior. The maximum load was attained at engineering strains in the range 0.7 to 1.3 (depending on the strain rate) after a marked nonlinear region which followed the fiber behavior at high temperature. Moreover, localization of damage did not occur after the peak load. Final failure took place through the progressive necking of the specimen up to the formation of a thin filament of parallel fibers while the fiber network was disentangled. This behavior was favored by the softening of the interfiber bonds, which favored the spread of the damage throughout the specimen as opposed to localization. As a result of these mechanisms, the strength of the fabric was much smaller and the energy absorption capability increased slightly. The specimens tested at ambient temperature presented an intermediate behavior between those tested at 248 and 383 K.

In summary, fiber properties and interfiber bond strength determined the mechanical performance of thermally-bonded PP nonwoven fabrics. The former controlled the behavior before the maximum load, including the extent of the nonlinear region, while the latter determined the post-peak behavior. Brittle interfiber bonds promoted the localization of damage and reduced the strain-to-failure as well as the energy absorbed during deformation, while the softening of the interfiber bonds at high temperature inhibited the localization of damage and enhanced the strain to failure.

Acknowledgment

This investigation was supported by the Spanish Ministry of Economy and Competitiveness through the Project MAT2012-37552.

References

Badel, P., Vidal-Salle, E., Maire, E., Boisse, P., 2008. Simulation and tomography analysis of textile composite reinforcement deformation at the mesoscopic scale. Compos. Sci. Technol. 68.

Boubaker, B., Haussy, B., Ganghoffer, J.F., 2007. Discrete models of woven structures. Macrosc. Approach. Compos. Part B Eng. 38, 498–505.

Bronkhorst, C.A., 2003. Modelling paper as a two-dimensional elastic-plastic stochastic network. Int. J. Solids Struct. 40, 5441–5454.

Cao, J., Akkerman, R., Boisse, P., Chen, J., Cheng, H., de Graaf, E.F., Gorczyca, J.L., Harrison, P., Hivet, G., Launay, J., Lee, W., Liu, L., Lomov, S.V., Long, S., de Luycker, E., Morestin, F., Padvoiskis, J., Peng, X.Q., Sherwood, J., Stoilova, T., Tao, X.M., Verpoest, I., Willems, A., Wiggers, J., Yu, T.X., Zhu, B., 2008. Characterization of mechanical behavior of woven fabrics: experimental methods and benchmark results. Compos. Part A Appl. Sci. Manuf. 39, 1037–1053.

Durville, D., 2010. Simulation of the mechanical behaviour of woven fabrics at the scale of fibers. Int. J. Mater. Form. 3, 1241–1251.

Farukh, F., Demirci, E., Sabuncuoglu, B., Acar, M., Pourdeyhimi, B., Silberschmidt, V.V., 2013. Characterisation and numerical modelling of complex deformation behaviour in thermally bonded nonwovens. Comput. Mater. Sci. 71, 165–171.

Hägglund, R., Isaksson, P., 2006. Analysis of localized failure in low-basis weight paper. Int. J. Solids Struct. 43, 5581–5592.

Hou, X., Acar, M., Silberschmidt, V.V., 2009. Tensile behavior of low density thermally bonded nonwoven material. J. Eng. Fibers Fabr. 4, 26–33.

Hou, X., Acar, M., Silberschmidt, V.V., 2011. Finite element simulation of low-density thermally bonded nonwoven materials: effect of orientation distribution function and arrangement of bond points. Comput. Mater. Sci. 50, 1292–1298.

Isaksson, P., Dumont, P.J.J., Roland de Roscoat, S., 2012. Crack growth in planar elastic fiber materials. Int. J. Solids Struct. 49, 1900–1907.

Isaksson, P., Gradin, P., Kulachenko, A., 2006. The onset and progression of damage in isotropic paper sheets. Int. J. Solids Struct. 43, 713–726.

Isaksson, P., Hägglund, R., 2009. Strain energy distribution in a crack-tip region in random fiber networks. Int. J. Fract. 156, 1–9.

Isaksson, P., Hägglund, R., Gradin, P., 2004. Continuum damage mechanics applied to paper. Int. J. Solids Struct. 41, 4731–4755.

Jubera, R., 2013. Experimental characterization of the tensile mechanical behavior of a polypropylene geotextile (master thesis). Universidad Politécnica de Madrid.

Khan, M., Mabrouki, T., Vidal-Salle, E., Boisse, P., 2010. Numerical and experimental analyses of woven composite reinforcement forming using a hypoelastic behaviour. application to the double dome benchmark. J. Mater. Process. Technol. 210, 378–388.

Kulachenko, A., Uesaka, T., 2012. Direct simulations of fiber network deformation and failure. Mech. Mater. 51, 1–14.

Lomov, S.V., Ivanov, D.S., Verpoest, I., Zako, M., Kurashiki, T., Nakai, H., Hirosawa, S., 2007. Meso-fe modelling of textile composites: road map, data flow and algorithms. Compos. Sci. Technol. 67, 1870–1891.

Rawal, A., Lomov, S., Verpoest, I., 2008. An environmental scanning electron microscope study of a through-air bonded structure under tensile loading. J. Text. Inst. 99, 235–241.

Rawal, A., Priyadarshi, A., Kumar, N., Lomov, S., Verpoest, I., 2010. Tensile behaviour of nonwoven structures: comparison with experimental results. J. Mater. Sci. 45, 6643–6652.

Ridruejo, A., González, C., LLorca, J., 2010. Damage micromechanisms and notch sensitivity of glass-fiber non-woven felts: an experimental and numerical study. J. Mech. Phys. Solids 58, 1628–1645.

Ridruejo, A., González, C., LLorca, J., 2011. Micromechanisms of deformation and fracture of polypropylene nonwoven fabrics. Int. J. Solids Struct. 48, 153–162.

Ridruejo, A., González, C., LLorca, J., 2012. A constitutive model for the in-plane mechanical behavior of nonwoven fabrics. Int. J. Solids Struct. 49, 2215–2229.

Russell, S., 2007. Handbook of Nonwovens. The Textile Institute. Woodhead Publishing Ltd.
Silberstein, M.N., Pai, C.L., Rutledge, G.C., Boyce, M.C., 2012. Elastic-plastic behavior of non-woven fibrous mats. J. Mech. Phys. Solids 60, 295–318.
Totry, E., González, C., LLorca, J., Molina-Aldareguía, J.M., 2009. Mechanisms of shear deformation in fiber-reinforced polymers: experiments and simulations. Int. J. Fract. 158, 197–209.
Totry, E., Molina-Aldareguía, J.M., González, C., LLorca, J., 2010. Effect of fiber, matrix and interface properties on the in-plane shear deformation of carbon-fiber reinforced composites. Compos. Sci. Technol. 70, 970–980.
Wilbrink, D.V., Beex, L.A.A., Peerlings, R.H.J., 2013. A discrete network model for bond failure and frictional sliding in fibrous materials. Int. J. Solids Struct. 50, 1354–1363.